CHAPTER 2

Modeling Research on Seasonal to Interannual Variability

The discovery in the 1980s of a significant extratropical impact of the tropical Pacific ENSO phenomenon, and the demonstration that several elements of the phenomenon could be predicted two or more seasons in advance using relatively simple models, were important developments in climate research. They rekindled interest in gaining a better understanding of ENSO dynamics, in the hope of making even better predictions. They also raised hopes that at least some aspects of interannual variability might be similarly predictable in other parts of the globe, not only from ENSO's remote impact but also through possibly predictable slow variations in other ocean basins. International research programs such as TOGA and CLIVAR were launched in pursuit of these hopes. Largely from their impetus, the observing system in the tropical Pacific was vastly improved, global gridded observational datasets spanning several decades were generated through various 'reanalysis' efforts, and extensive numerical simulations and predictions of interannual climate variations were undertaken with both uncoupled and coupled global climate models. Our understanding of the variability and predictability of the climate system on this time scale has matured considerably as a result. CDC has contributed significantly to the present store of knowledge in this area, and is at the forefront in addressing many of the remaining questions.

*CDC scientists have provided important evidence that the **predictable** evolution of ENSO and of the associated remote teleconnections are governed largely by **linear, low-dimensional** dynamics. This may be one reason why simple empirical linear models remain competitive with sophisticated GCMs at making seasonal predictions. Indeed the question of how much extratropical predictability exists on this scale beyond that associated with simple linear ENSO signals has become a recurring theme in CDC research. In the last four years, we have identified the situations in which the dynamics of ENSO are significantly nonlinear, clarified the extent to which the remote impacts can be nonlinear, and explored the extent to which those impacts might be sensitive to the details of the tropical SST anomaly patterns, i.e. be "higher-dimensional". We have also explored how the nonlinear and higher-dimensional dynamics might affect the tails of the probability distributions of atmospheric variables on synoptic, intraseasonal, and seasonal scales, and thus the risk of extreme anomalies on those scales. We have investigated the predictability of SSTs in other oceans basins, both through "atmospheric bridge" ENSO teleconnections and through the year-long persistence and subsequent re-emergence of SST anomalies from below the seasonally-varying surface mixed layer. We have also continued to assess the impact of such SSTs on the atmospheric circulation.*

2.1 Understanding and predicting seasonal tropical SST variations

CDC scientists have pioneered the development of Linear Inverse Modeling (LIM) as a diagnostic and forecasting tool. LIM is a method of extracting the dynamical parameters of a system from data. The assumption is made that the dynamics can be modeled as a stable linear multivariate process driven by geographically coherent white noise. The estimated dynamical parameters can then be used to make forecasts of the system. Real-time seasonal LIM forecasts of tropical Indo-Pacific SST anomalies are published monthly in the *Climate Diagnostics Bulletin* and quarterly in the

Experimental Long-Lead Forecast Bulletin (ELLFB). They are also available through CDC's website at http://www.cdc.noaa.gov/~lem/IndoPacific.frcst.html.

An important original result from our LIM diagnosis of Indo-Pacific SST variability was the identification, through a singular-vector analysis of the empirically-determined system propagator, of an *optimal initial SST pattern* for SST anomaly growth over 7 months in the basin. This structure evolves in 7 months into a pattern resembling a mature ENSO event (**Fig. 2.1**), and may therefore be viewed as a dynamically relevant precursor to ENSO. And indeed, as **Fig. 2.2**. shows, whenever an SST anomaly pattern projects appreciably on this structure, there is a good chance of obtaining large SST anomalies in the Niño 3.4 area 7 months later. **Figure 2.2** also shows that the projection statistics are similar whether they are evaluated for a time period including the training period (COADS data: 1950–1990) or for independent data (NMC Real-time Surface Marine data: 1991–2001). Encouraged by this robust behavior, we now provide real-time monitoring of the projection of the SST anomaly field on this structure through our website at http://www.cdc.noaa.gov/~lem/opt/optstr.html.

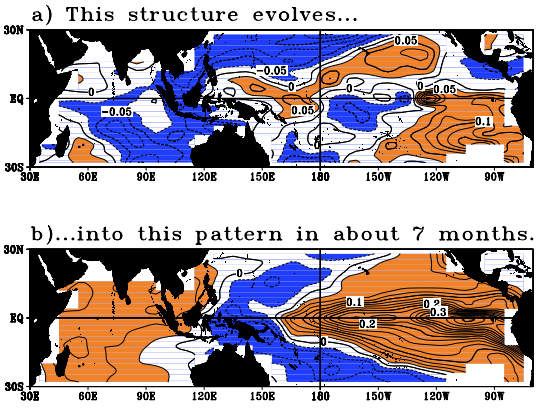

Fig. 2.1 (a) The optimal initial structure for SST anomaly growth. The pattern is normalized to unity. The contour interval is 0.025. Loadings greater than 0.025 are colored red; dashed lines indicate negative contours. **(b)** The pattern predicted when the pattern in (a) is used as the initial condition.

We have also recently published procedures for estimating improved confidence intervals on our SST forecasts. Until recently, the confidence intervals were those appropriate to our assumed stationary linear Markov process; that is, they showed the expected forecast error of a stable linear model driven by stationary white noise. The improved error bars also include estimated contributions from our neglect of the seasonal variation of the stochastic forcing, from estimating the model's parameters in a training period of finite length, and from initial condition errors.

The actual forecast error normalized by the rms of the total expected error estimated in this manner (**Fig. 2.3**) shows how much better the forecast skill is during La Niña than El Niño. This is consistent with our conclusion, stated in several papers, that nonlinear dynamics become important during the warmest phase of warm events. We have continued to investigate the failure of LIM during such periods. Although the lack of skill is mostly due to the greater importance of nonlinearity, an interesting recent finding was that LIM would nevertheless have been useful during late 1994–early 1995 had it been applied to *weekly* instead of seasonal SSTs. Evidence has also been found that unpredictable sto-

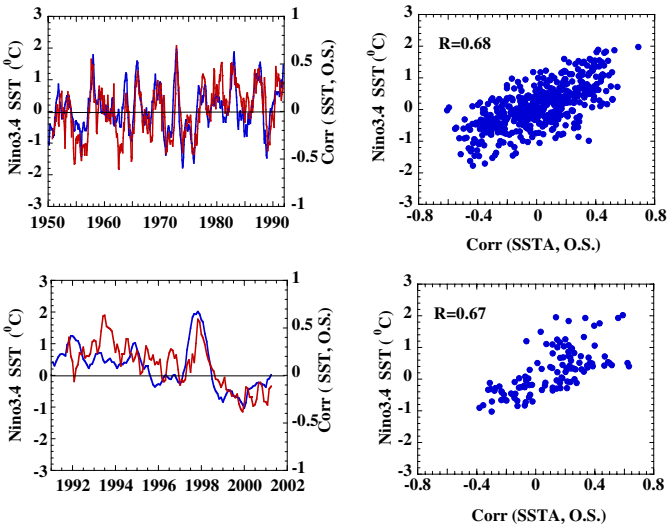

Fig. 2.2 Left panels: Time series of SST anomaly in Niño 3.4 (blue line), and the pattern correlation of the SST anomaly pattern seven months earlier with the optimal structure (red line). The information in these left panels is also displayed in the form of scatter plots in the right panels.

chastic forcing accounted for a large portion of the observed warming during the strong 1997–1998 event.

CDC also provides LIM forecasts of the tropical north Atlantic and Caribbean SSTs in the *ELLFB*. Again, these forecasts are available through our website at http://www.cdc.noaa.gov/~lem/Atlantic.forecast.html. We have shown that forecast skill in these Atlantic regions is related to the skill of predicting El Niño. We have also used LIM to diagnose the dynamical nature of tropical Atlantic SST variability, and published evidence that the familiar "dipole" SST anomaly pattern is a dynamically realizable structure (as opposed to merely the dominant EOF of regional SST variability), but whose development is often interrupted by ENSO influences from the east Pacific.

Our original claim that the basic dynamics of ENSO are stable, linear and stochastically forced has been independently confirmed by others and is gradually forcing a paradigm shift in this field. We have continued investigating

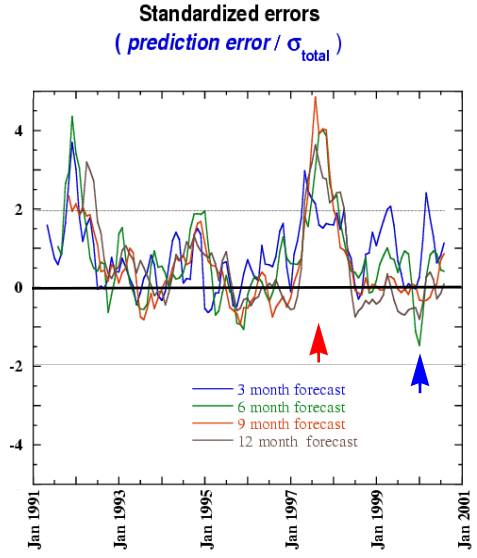

Fig. 2.3 Time series of actual LIM forecast errors normalized by one standard deviation of the total forecast uncertainty. The horizontal lines at ± 1.96 indicate the 95% confidence interval. The red and blue arrows indicate prominent El Niño and La Niña events during this period.

the dynamical nature of ENSO, especially in collaboration with scientists at Texas A&M University. A recently published study showed that an intermediate coupled ENSO-prediction model of the Cane-Zebiak type, tuned to be in a stable stochastically forced regime, generated more realistic SST variability than did the same model tuned to give self-sustained oscillations.

2.2 Understanding and predicting the global impact of tropical SST variations

CDC scientists are using a combination of observational and general circulation modeling approaches to address this problem. The observational studies rely heavily on the 50-year NCEP reanalysis dataset. The GCM studies are conducted by running various versions of the NCEP and GFDL global atmospheric models with prescribed SST forcing, in some cases by coupling to a mixed layer in parts of the world ocean. We have also analyzed 10–12 member ensembles of 50-year runs made by several GCM groups (NCEP, GFDL, NCAR, ECHAM, IRI) with prescribed observed SST forcing, generally for the period 1950–1995, prescribed either globally or in the tropics.

2.2.1 Prediction skill and predictability

Outside the tropics, SST-forced signals account for a relatively small (generally less than 25%) portion of extratropical variability on seasonal to interannual scales. This fundamentally limits the average skill of a deterministic (as opposed to a probabilistic) seasonal forecast, regardless of whether it represents the mean of a large forecast ensemble or even a multi-model ensemble. The limitation arises from a generally small signal-to-noise ratio, and cannot be overcome by improving models. The noise is associated with chaotic (i.e., unpredictable) nonlinear interactions and is intrinsic to the extratropical atmosphere. Still, in extreme individual cases, the signal can exceed the noise, making relatively skillful forecasts possible.

There are two other confounding factors that make it difficult for even sophisticated GCMs to improve upon the forecast skill of simple statistical models based on linear correlations between tropical SST and extratropical circulation anomalies. The first is the approximate linearity of the remote response to ENSO. The other is the relative *insensitivity* of that response to details of the tropical SST forcing; it appears that knowledge of the area-averaged anomaly in Niño-3.4 alone is almost enough.

Figure 2.4 provides a good illustration of these points. It shows the correlation of observed JFM-mean 200 mb geopotential height anomalies with those predicted, over a 26-year period, using two forecasting systems of vastly different complexity. The top panel shows the skill of a 9-member ensemble-mean forecast by the NCEP atmospheric GCM forced with observed concurrent SST anomalies in the tropical Pacific between 20°N and 20°S. Consistent with many studies, the correlation of the observed and predicted height anomalies is high in the tropics, and appreciable over North America and the northeast and southeast Pacific

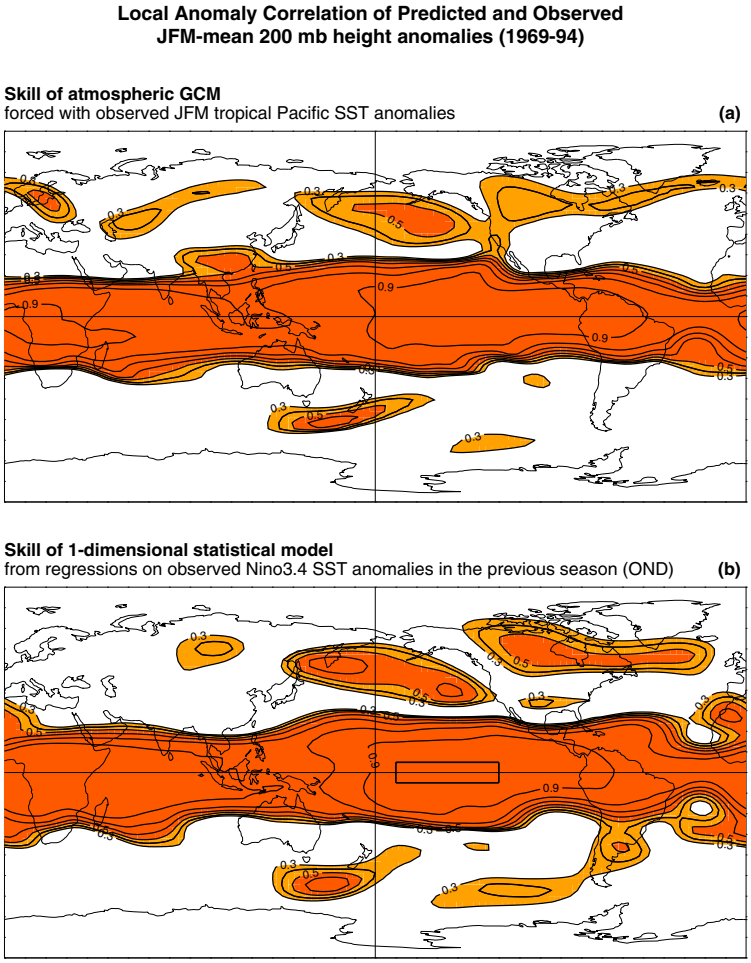

Fig. 2.4. Wintertime 200 mb height seasonal forecast skill of (a) the NCEP atmospheric GCM with specified observed SSTs in the tropical Pacific basin and (b) a simple linear regression model based on seasonal 200 mb height correlations with Niño 3.4 SSTs. See text for details.

oceans. This is encouraging, although it should be noted that the GCM forecasts are not true forecasts. Still, they give an idea of the potential predictability of seasonal anomalies around the globe if the tropical Pacific SSTs were to be predicted accurately. The surprise in **Fig. 2.4** is the lower panel. It shows the skill of the simplest conceivable linear regression forecasts for the same cases as in the upper panel, using the regression coefficients of observed JFM 200 mb height anomalies against the area-averaged observed JFM SST anomaly in Niño-3.4. The forecasts themselves are made using the observed Niño-3.4 SST anomaly in the *previous* 3-month period (OND) as the predictor. These simple forecasts are clearly comparable in skill to the GCM forecasts. They also represent legitimate 1-season 'coupled model' forecasts, in that they incorporate a trivial persistence forecast of the Niño-3.4 SST anomalies from OND to JFM.

The rough agreement between the two panels in **Fig. 2.4** may be interpreted as reflecting either true seasonal predictability limits or the need for further GCM improvement. There is room for both interpretations, although we are more inclined toward the former. GCM error is probably not the main culprit here: several other GCMs analyzed by us yield skill patterns very similar to that in the upper panel. Also, when the NCEP GCM is asked to predict its own behavior, such as when using an 8-member ensemble-mean to predict the 9th member's seasonal anomalies, its skill is again similar to that in the upper panel. One can thus make a case that the modest extratropical values in **Fig. 2.4** are mainly a reflection of the limited intrinsic predictability of extratropical seasonal averages associated with tropical SST forcing. As mentioned earlier, this in turn is mainly due to a modest signal-to-noise ratio.

CDC scientists have attempted to clarify the relationship between the expected anomaly correlation skill ρ of ensemble-mean forecasts and the signal-to-noise ratio *s*, defined as the ratio of the ensemble-mean anomaly to the ensemble spread. **Figure 2.5** summarizes this general relationship, which is useful in interpreting many GCM results. The ρ_∞ and ρ_1 curves show the expected skill of infinite-member and single-member ensemble-mean forecasts with a perfect model. The third (blue) curve depicts the expected skill of infinite-member ensemble-mean forecasts with an imperfect model, whose systematic error s_e (i.e., its error in determining the true *s*) is of the same magnitude as *s*. Note that these curves are applicable to any forecast variable, in any forecasting situation, and to any forecasting method, including the regression method used in **Fig. 2.4b**.

The ρ_∞ curve represents a hard predictability limit with a perfect model, and shows that to produce 'useful' forecasts with anomaly correlations greater than 0.6, *s* needs to be greater than 0.75. To produce 'excellent' forecasts with anomaly correlations greater than 0.9, *s* needs to be greater than 2. Given the evidence from several studies that *s* for ENSO-related 200 mb seasonal height anomalies is approximately between 0.5 and 1 in the extratropical Pacific-American sectors of both hemispheres, and greater than 2 in the tropics, the results in **Fig. 2.4** are not surprising. **Figure 2.5** is also useful for assessing to what extent the modest skill in **Fig. 2.4a** might be due to model error or using only 9-member ensembles. The difference between ρ_∞

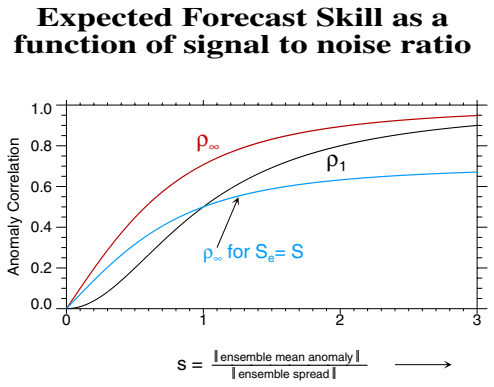

Fig. 2.5 Expected anomaly correlation forecast skill of ensemble-mean forecasts as a function of signal to noise ratio *s*. The red curve is the expected skill of an infinite-member forecast, the black curve the expected skill of a single-member forecast. The blue curve shows the expected skill of an infinite-member ensemble forecast using an imperfect model whose standardized systematic error is of the same magnitude as *s*.

and ρ_1 shows the potential gain in skill by using infinite-member ensembles instead of a single member. The maximum gain is 0.25, for $s \sim 0.6$. However, most of this gain is attainable with about 25 members, and even a ρ_9 curve (not shown) is close to the ρ_∞ curve. The loss of skill due to model error (blue curve) is probably of greater concern in **Fig. 2.4a** than not having enough members. However, model error could equally be affecting skill in **Fig. 2.4b**.

2.2.2 New research challenges

Figures 2.4 and **2.5** together suggest that the modest skill, on average, of deterministic extratropical seasonal forecasts is largely consistent with the predictability limits imposed by the modest local values of *s* associated with the tropically forced signal. Given also the evidence in **Fig. 2.4b** that similar skill can also be achieved with simple linear regression models, the question naturally arises as to what further useful predictive information can be extracted by running GCM ensembles.

CDC scientists have spent considerable time pondering this issue, and have come up with several encouraging possibilities. In one way or another, they all involve focusing on the distributional aspects of the ENSO response rather than on the ensemble-mean. For example, as **Fig. 2.6a** shows, a modest shift in the mean of 0.5 (in units of standard deviation), while not large enough to affect appreciably the expected seasonal mean of an extratropical variable, can still greatly affect the probability of its extreme values. The risk of obtaining an extreme positive value of greater than +1 increases from 16% to 31%, and the risk of obtaining an extreme negative value decreases from 16% to 7%. Thus without ENSO the risks of extreme positive and negative anomalies are the same, but with ENSO, even for a modest *s* of 0.5, the risk of an extreme positive anomaly becomes 4.4 (=31/7) times the risk of an extreme negative anomaly. **Figure 2.6b** shows how this risk ratio can be equally strongly affected by modest changes of noise. In this example, a 20% reduction of standard deviation combined with a mean

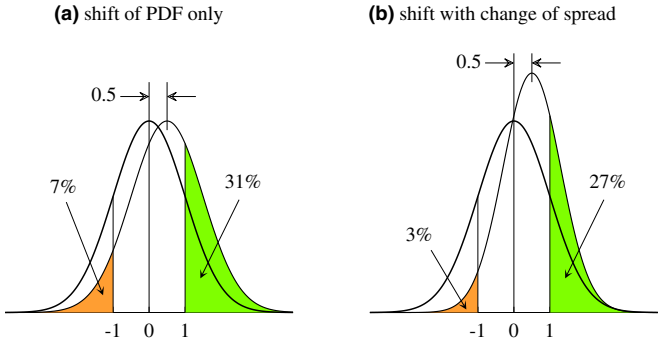

Fig. 2.6. (a) An illustration of how a mean shift of 0.5 of a normal distribution increases the probability of extreme positive values from 16% to 31% and decreases the probability of extreme negative values from 16% to 7%. **(b)** Illustration of the altered probabilities of extreme values when the mean shift of 0.5 is also accompanied by a reduction of the standard deviation from 1 to 0.8.

shift of 0.5 changes the risk ratio from 1 (=16/16) to 9 (=27/3).

When even minor PDF shifts and changes of variance imply large changes in the risks of extremes values, determining them accurately becomes important. It is easy to see how a good GCM might have an advantage over the regression model of **Fig. 2.4b** in this regard, whose parameters cannot be estimated accurately enough from the limited observational record to have confidence in its predictions of extreme values. Further, one can run as many GCM ensemble members as necessary in individual forecast cases to predict the changes of extreme risks within specified confidence intervals. The regression-model also assumes, in effect, that ENSO-induced mean PDF shifts are strictly linear with respect to the SST forcing and that there are no changes of noise, or variability. CDC scientists have spent considerable effort on ascertaining the extent to which such assumptions are valid, since they have a large bearing on the problem at hand.

2.2.3 Understanding the sensitivity of the atmospheric response to details of the anomalous SST forcing

The regression-model used in **Fig. 2.4b** always predicts the same signal pattern of the global atmospheric response; only its amplitude varies from forecast case to case in direct proportion to the strength of the Niño 3.4 SST anomaly. As we have seen, this doesn't seem to affect its deterministic forecast skill overmuch, but the question is whether it limits predictions of the risk of extreme anomalies. To what extent does the remote SST-forced signal vary from case to case? To what extent are its variations determined by the nonlinearity of the response to the amplitude and sign of the SST forcing in Niño 3.4, and to what extent by the details of the SST anomaly pattern in the wider tropical Indo-Pacific domain? We have conducted several studies to answer these questions.

Figure 2.7 gives a sense of the signal variation from case to case. Sampling uncertainty is an issue in this problem, given that the number of samples required to establish that s is statistically different from zero is inversely proportional to the *square* of s. At the 5% level, the number of samples should be greater than $8/s^2$. To establish the significance of $s = 0.5$ thus requires 32 samples; to establish the significance of *changes* of s from case to case, say of order 0.25, would require many more, 128. With this in mind, we ran a very large 180-member seasonal ensemble with the NCEP atmospheric GCM with prescribed observed global SST forcing corresponding to the El Niño of 1987, and another 180-member ensemble for the La Niña of 1989. The right-hand panels of **Fig. 2.7** show the ensemble-mean 500-mb height anomalies obtained in these integrations (defined with respect to the ensemble-mean obtained in another set of 180 integrations with climatological-mean SST forcing). To our knowledge this is the most statistically confident determination of the global SST-forced signal ever made for two different observed SST forcing patterns. Note that the sign of the response has been reversed in the lower panel for easier comparison with the

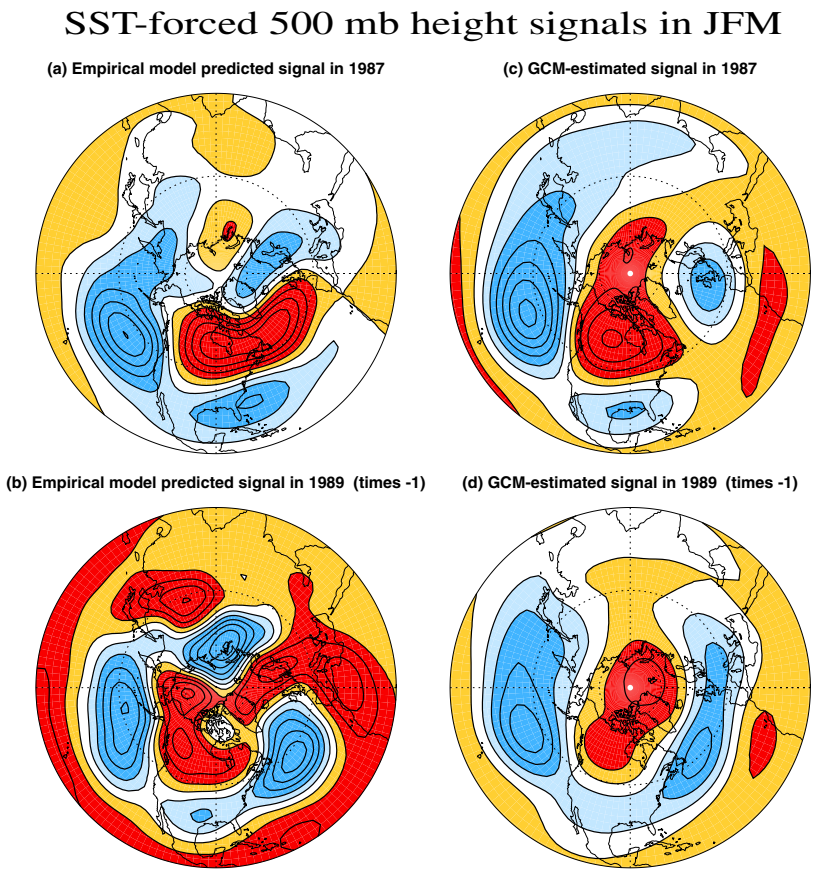

Fig. 2.7 The SST-forced signal in 500 mb heights during the El Niño winter of JFM 1987 (top panels) and the La Niña winter of JFM 1989 (bottom panels, with sign reversed) estimated by a GCM (right panels) and an empirical method (left panels). The right panels show the ensemble-mean anomaly fields obtained in 180 seasonal integrations of the NCEP AGCM with prescribed global SST forcing during JFM 1987 and JFM 1989. The left panels show scaled historical composite 500 mb anomaly fields derived from 10 observed El Niño and 10 observed La Niña events in the 1958–1999 period, defined with respect to a Niño 3.4 SST anomaly index. The composite patterns were scaled by factors of 0.73 and 1.36 to account for the moderate Niño 3.4 index magnitude during 1987 and the larger magnitude during 1989, respectively. The contour interval is 10 m in all panels. Positive values are indicated by red and negative by blue shading.

upper panel. For comparison we also show in the left panels, in an identical format, observational 500-mb composite anomaly patterns for 10 El Niño and 10 La Niña events based on the Niño 3.4 index, and defined with respect to 10 "neutral" events. Note that the *amplitudes* of these composite patterns have been scaled by 0.73 and 1.36, in proportion to the observed Niño 3.4 SST anomaly magnitudes during the moderate 1987 El Niño and the strong 1989 La Niña events, respectively. Thus these left panels may be interpreted as the SST-forced 500-mb height signals during 1987 and 1989 as predicted by an empirical method. This method is superior, in principle, to that used in **Fig. 2.4b** in that it predicts different response patterns in

El Niño and La Niña cases, as shown here.

Although the GCM's signal patterns for these individual El Niño and La Niña winters are generally similar to one another, there are some notable differences. The El Niño response is stronger in the PNA sector, despite the weaker SST forcing. This is also true in the empirical forecast. There is little else to compare between the GCM and empirical forecasts because of sampling uncertainty in the empirical forecasts, i.e., the fact that the left panels are derived from only 10 cases each in the historical record. In areas such as the North Atlantic where the left panels predict a strong asymmetric signal of the same sign in 1987 and 1989, the significance of that asymmetry is therefore questionable. The differences between the GCM's predicted signal patterns for 1987 and 1989 are much more reliable in this regard, and though more modest, are large enough that they would have had important implications for predicting the risks of extreme anomalies during these winters.

There is thus evidence of significant signal variation from case to case. To put these results on a stronger footing, one might ideally wish to generate similar 180-member ensembles for each one of the past 50 or so winters. This has not yet been done. However, results from a 46-member multi-model ensemble of four different atmospheric GCMs (NCAR CCM3, NCEP, GFDL, and ECHAM) offer additional evidence of the existence of different response patterns. Between 10 and 12 member ensembles were gen-

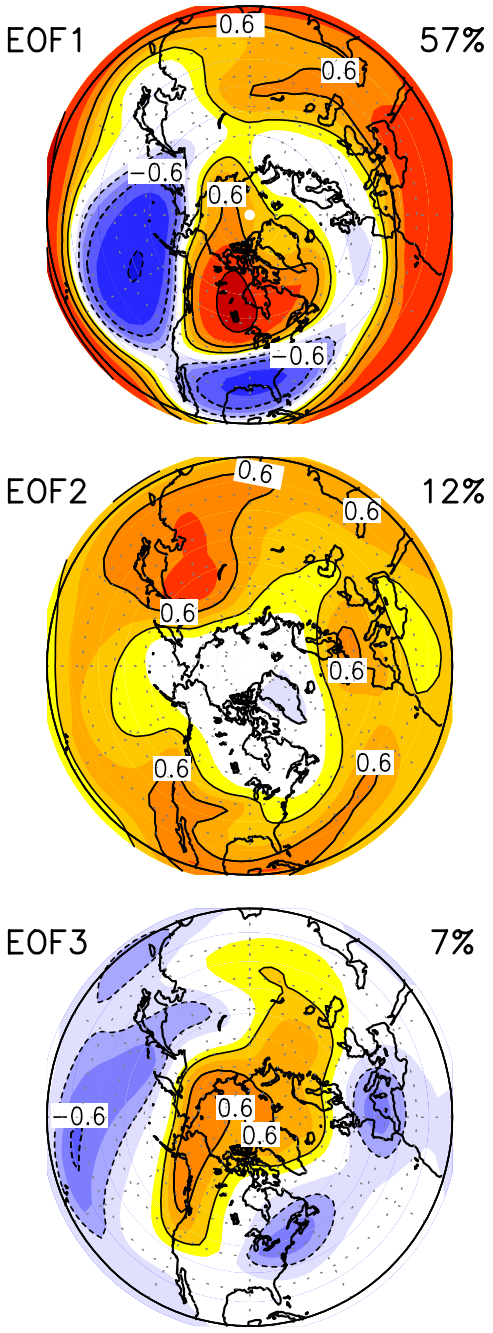

Fig. 2.8 The first three EOFs of SST-forced 500 mb height signals in a multi-GCM ensemble of 50-year integrations made with prescribed evolving observed global SST boundary conditions. See text for further details. The values plotted are the correlations of the EOF's Principal Component time series with the local 500 mb height time series of the SST-forced signal. Positive values are indicated by red and negative by blue shading.

erated for each model forced with identical evolving observed global SSTs over the past 50 years. For each one of the 50 winters, the SST-forced signal at 500 mb was defined as a weighted average of the ensemble-mean responses of the 4 GCMs. Finally, an EOF analysis of these 50 signal patterns was performed. **Figure 2.8** shows the first three EOFs, together with their fractions of the total signal variance explained. The leading EOF alone accounts for 57% of the global signal variance, and as much as 80% over the PNA region. Most elements of this pattern are evident in all the four panels of **Fig. 2.7**. The dominance of this signal pattern, its strong similarity to the classic observed ENSO teleconnection pattern, and also to the unchanging forecast pattern of the regression model used in **Fig. 2.4b**, explains why the upper and lower panels of **Fig. 2.4** are so similar. Still, there is evidence in **Fig. 2.8** of apparently minor but potentially important deviations from this dominant signal pattern from winter to winter. The second EOF is largely zonally symmetric, with out-of-phase anomalies in polar and subtropical latitudes. Locally, it explains a substantial fraction of the signal variability in the subtropics, and its associated Principal Component (PC) time series describes a tropospheric warming trend of lower latitudes over 1950–1999 associated with a long-term tropical SST warming trend. The third EOF resembles a tropically forced wavetrain with centers spatially shifted relative to those of the leading EOF. Its PC time series regressed on the simulated tropical precipitation fields yields a regression map with appreciable magnitudes in the western and central equatorial Pacific. This third EOF may thus reflect a genuine sensitivity of the SST-forced extratropical signal to variations of the anomalous tropical SST pattern from winter to winter.

It should be stressed that the GCM results in **Figs. 2.7** and **2.8** are all for global SST forcing. To what extent can the signal variation evident in these figures be attributed strictly to the *tropical Pacific* SST forcing, in particular to asymmetric responses to El Niño and La Niña forcing? There is a strong suggestion of a weaker response to La Niña forcing in the lower panels of **Fig. 2.7**. Such a weaker response (not shown) is also clearly evident in the composite El Niño and La Niña signals in the 4 different ensemble GCM simulations for 1950–1995 described above. Are there also significant differences in the *patterns* of the response? To what extent do they contribute to the third EOF in **Fig. 2.8**? Several CDC studies have attempted to address such questions cleanly, by examining the atmospheric response to the first EOF pattern of tropical Pacific SST (very similar to the Pacific portion of the lower panel of **Fig. 2.1**) with positive ("El Niño") and negative ("La Niña") signs. A weaker response to the negative EOF forcing has indeed been confirmed, but is appreciable only for large amplitude forcing.

Figure 2.9 shows results from a GCM experiment designed specifically to address this issue. A 9-member NCEP GCM ensemble was generated for 1963–1989 by forcing throughout the 27 years with the first SST EOF pattern, varying

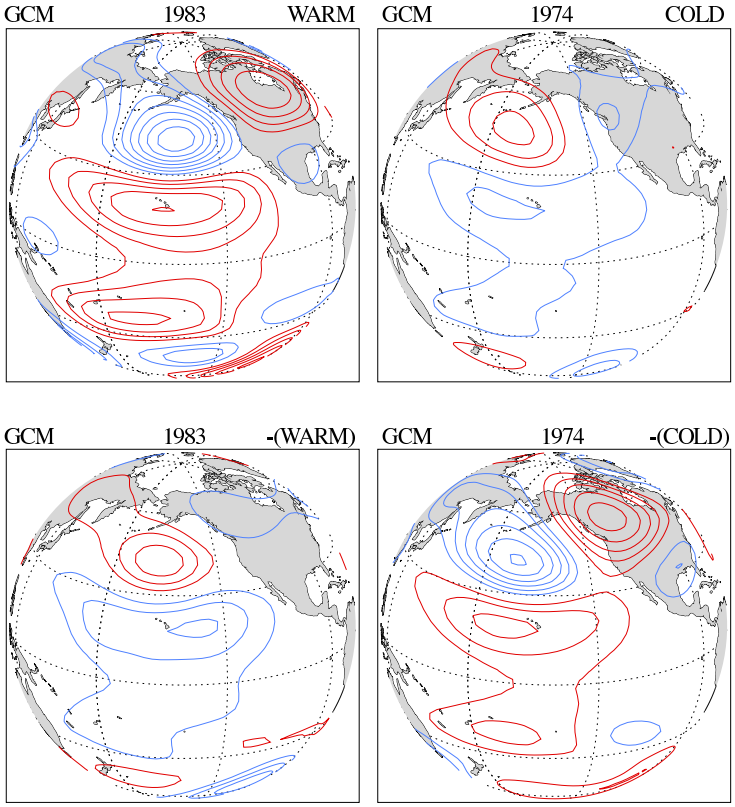

Fig. 2.9 GCM 200 mb height responses in northern winter (DJF) to the first EOF pattern of tropical Pacific SST forcing, with the observed amplitude during DJF 1982/83 (upper left panel), the observed amplitude during DJF 1973/74 (upper right), the negative of the observed amplitude during DJF 1982/83 (lower left), and the negative of the observed amplitude during DJF 1973/74 (lower right). The contour interval is 10 m. Positive values are indicated by red and negative by blue contours. See text for further details.

in magnitude and sign as its associated PC time series. The upper panels of **Fig. 2.9** show the ensemble-mean responses during the strongest warm and cold winters of 1983 and 1974, respectively, in this period. The response is clearly weaker for the 1974 event. This is suggestive but not conclusive, since the magnitude of the SST forcing was also weaker in 1974. To settle this, the entire experiment was repeated with the sign of the PC time series reversed. The ensemble-mean responses for the sign-reversed 1983 and 1974 winters are shown in the lower panels. The 1974 response is now stronger than the 1983 response, despite the weaker magnitude forcing. We had noted this effect earlier in **Fig. 2.7**, but the result here is cleaner. It confirms that the remote atmospheric response to the tropical Pacific SST forcing is appreciably stronger for strong warm than for the strong cold SST forcing. A top-to-bottom comparison in **Fig. 2.9** compares the responses to the same SST forcing but of

opposite sign, and further confirms this result.

2.2.4 ENSO-induced changes of variability

To what extent does ENSO affect the atmospheric noise (i.e., the variability) as hypothesized in **Fig. 2.6b**? We have addressed this issue in several recent publications. In one study, we examined the standard deviation of seasonal-mean 500 mb heights in our 180-member GCM ensembles for the winters of 1987 and 1989, and found a modest overall increase in the warm (1987) and a decrease in the cold (1989) ensemble compared to that in the neutral 180-member ensemble. This was speculated to be forced partly by the increased variability of seasonal precipitation in the warm (and decreased variability in the cold) ensemble in the Niño-4 area of the central equatorial Pacific, which has been shown to be sensitive region for forcing a large global circulation response. Another study searched for ENSO-induced changes of seasonal noise in the smaller AMIP-style GCM ensembles used in **Fig. 2.8**, but found little impact in the PNA region. While these findings seem to conflict, a closer look at the published figures shows that the results are not inconsistent in the PNA region. To the extent that the altered extratropical noise is due to the tropical precipitation noise, the effect is also probably both GCM-dependent and ENSO event-dependent. It should be mentioned that sampling uncertainty is of even greater concern here than in **Figs. 2.7** and **2.8**. The number of samples required to establish the significance at the 5% level of a fractional change Δ of an ensemble's standard deviation is close to $3/\Delta^2$. To establish the significance of the Δ of 0.2 (corresponding to a 20% change of standard deviation) in **Fig. 2.6b** would thus require 75 samples from both the neutral and altered distributions. Any change of smaller than 17.5% would require more than 100 samples.

The effect of ENSO on *subseasonal* extratropical variability is equally important, and somewhat easier to establish. These effects can be distinct from the effects on seasonal mean quantities, and can have important practical implications. For instance, one may imagine a situation in which El Niño alters the occurrence of both cold waves and warm spells in a winter. The effect is a meaningful change in the risk of extreme weather, even though little seasonal mean signal might be evident. The few published studies on this topic, constrained either by sampling requirements or data availability, have formed composites over several ENSO events to diagnose the effect in limited regions. In an ambitious recent study, we have estimated the effect globally from our large AGCM ensembles for 1987 and 1989, and compared them with observational composites based on 11 El Niño and 11 La Niña events in the recent record. As in **Fig. 2.7**, the purpose of this comparison was to gauge to robustness of the changes of variability, their predictability, and their variation from event to event.

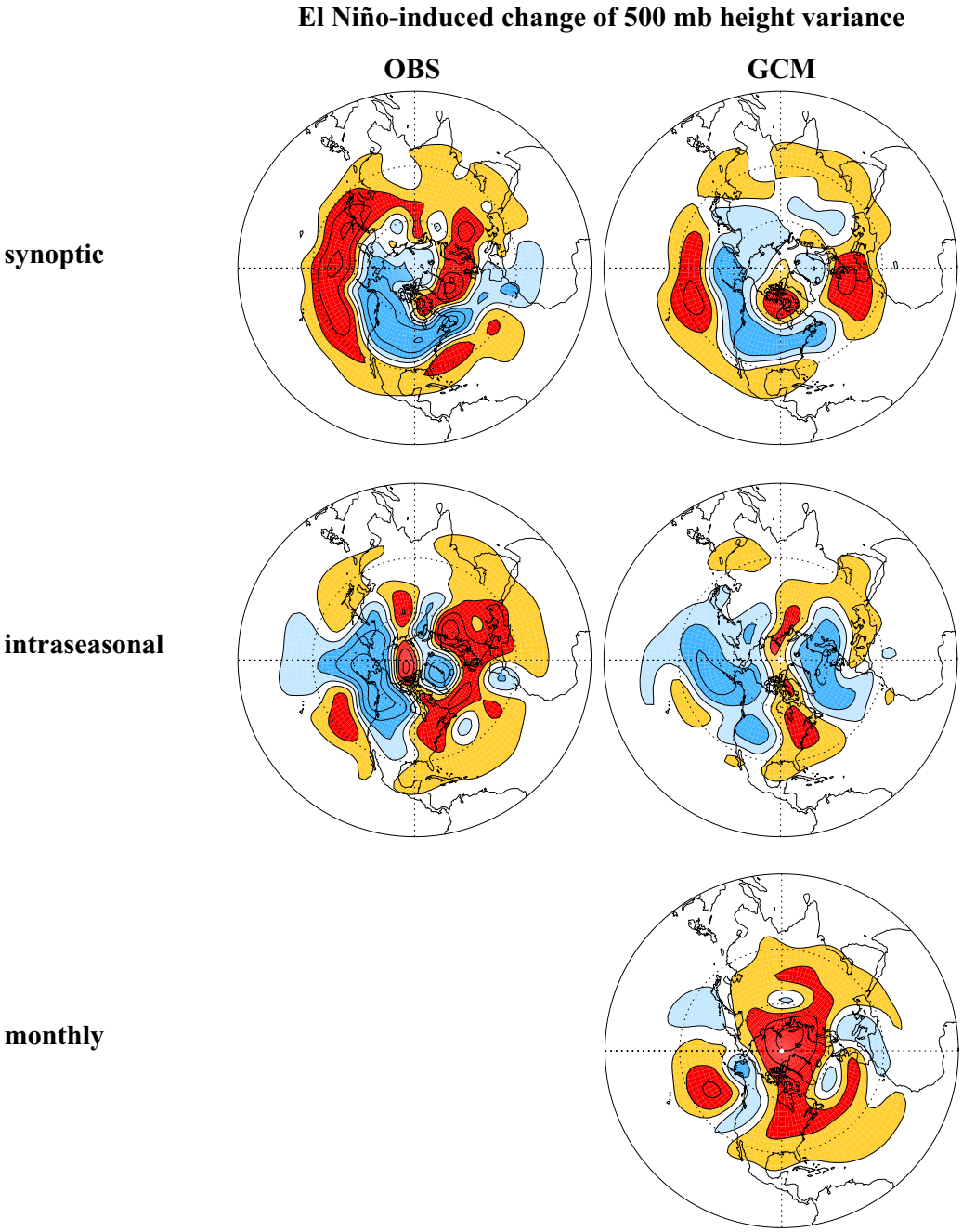

Fig. 2.10 El Niño-induced changes of variance on three different subseasonal time scales. The quantity plotted is the square root of the anomalous variance, with red shading for positive and blue for negative anomalous variance. The left panels are based on statistics averaged over 11 observed El Niño and 11 observed "neutral" JFM winters in the NCEP reanalysis dataset. The right panels are derived from a large AGCM ensemble with observed SST forcing for the El Niño winter of JFM 1987. Top panels: Synoptic scale (2 to 6 day periods), Middle panels: Intraseasonal scale (8 to 45 day periods.). Bottom panel: Monthly scale (30-day averages). Contours are drawn at 8 m intervals starting at 4 m in the top panels, and at 16 m intervals starting at 8 m in the middle and lower panels. See text for a fuller explanation.

The most important result from this analysis, depicted in **Fig. 2.10**, is that the patterns of the SST-forced anomalous height variability are markedly different for the synoptic (2 to 7 days), intraseasonal (8 to 45 days), and monthly (30 -day average) time scales. In contrast, the patterns of the anomalous tropical rainfall variability (not shown) are nearly identical across these time scales. **Figure 2.10** shows contours of Δ_σ , defined as the signed square root of the anomalous variance difference of 500 mb heights on these time scales (where by "signed" we mean that if the anomaly is negative, we depict its square root with a minus sign). The results for La Niña (not shown) are similar and generally of opposite sign. The comparison between the GCM and observational panels in **Fig. 2.10** is not clean. Nevertheless, their gross similarity is reassuring, both for the robustness of the changes of variability and this GCM's ability to simulate them. To that extent, their dissimilarity can be attributed to the comparison not being clean (i.e., event-to-event differences) and sampling error, especially in the observations (which is why the observational anomalous monthly variability map has been omitted).

The main ENSO effect on the synoptic scale is a southward shift of the storm track over the Pacific ocean and North America. On the intraseasonal scale, it is a decrease of height variance over the north Pacific, consistent with a tendency of reduced blocking activity during El Niño. On monthly (and seasonal) scales there is a suggestion of an overall increase of variance. Referring back to **Fig. 2.6b**, it is evident that these differing ENSO impacts on extratropical noise on different time scales have very different implications for the risks of extreme anomalies on these scales. We believe that three quite distinct dynamical mechanisms are responsible for these sharp differences, and are currently investigating them in a hierarchy of dynamical models.

2.3 Understanding the impact of extratropical SST variations

Despite many studies, the precise role of extratropical SST variations in the dynamics of atmospheric low-frequency variability remains unclear. Many atmospheric GCM experiments have been performed with prescribed extratropical SST anomalies to determine the atmospheric response to them. The results have been variable and confusing, not only because the response is weak and difficult to establish in short integrations, but also because it is sensitive to the precise location of the prescribed SST anomaly in relation to the atmospheric jet streams and their associated storm tracks. The largest extratropical SST anomalies tend to occur near the jets, and may be thought of as having a direct effect on the mean flow, and on the storm tracks through the change in the mean flow. The altered storm tracks can, however, feed back on the mean flow. This indirect effect can be very important, but is difficult for GCMs to represent accurately.

We have investigated these issues in a series of long NCEP AGCM runs with

prescribed extratropical SST forcing. In a previously published study, an idealized warm SST anomaly was imposed near the Kuroshio region of the northwest Pacific. The atmospheric response to this was radically different in perpetual January and perpetual February integrations of the GCM: a baroclinic response in January and a nearly equivalent-barotropic ridge response in February. To understand this, we used a linear model to investigate the response to the SST anomaly as the sum of the direct heating-induced component and the indirect eddy-driven component associated with the altered storm tracks. (A novel feature of this calculation was that the altered storm-track forcing specified in the linear model was specifically that induced by the heating altered mean flow, diagnosed using Whitaker and Sardeshmukh's storm-track model). This diagnosis confirmed the dominance of the eddy-driven component, forced mainly by the altered eddy-momentum fluxes, in determining the barotropic ridge response. Without the eddy forcing, the response to a shallow heat source associated with the warm SST anomaly was always baroclinic, with a trough near the surface and a ridge aloft and downstream. This explains the baroclinic response to extratropical SST anomalies obtained in many low-resolution GCMs, in which the simulated storm tracks and eddy momentum-fluxes are generally too weak: in such GCMs the SST-induced alterations of the storm track are also too weak. An equivalent-barotropic ridge response develops only if the storm track is altered sufficiently strongly that strong anomalous eddy-forcing is generated at the correct locations to reinforce the heating-induced upper-level ridge and offset the lower-level trough. In this way, the atmospheric response becomes sensitive to the characteristics of the storm track and the position of the SST anomaly relative to the storm track.

As an example, **Fig. 2.11** shows the linear model results for idealized shallow heat sources associated with warm extratropical SST anomalies imposed on the

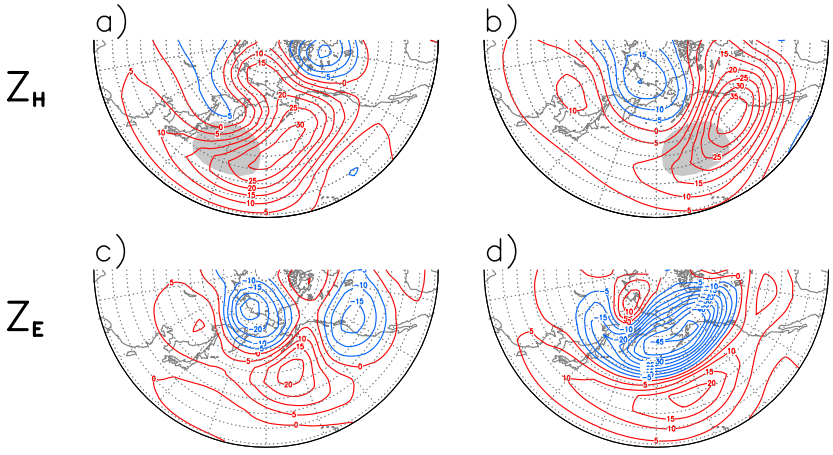

Fig. 2.11 A linear balance model's 250 mb geopotential height response in winter to a shallow elliptic heat source centered (a) at 40°N,160°E and (b) at 40°N,160°W. The model's height response to the anomalous eddy vorticity fluxes induced by these heat sources is shown in (c) and (d), respectively. The contour interval is 5 m; positive values are indicated by red and negative by blue contours.

observed winter-mean basic state. With an elliptic source specified over the western Pacific (left panels), the heating-induced upper-level ridge (upper panel) is reinforced by the eddy-driven equivalent-barotropic ridge (lower panel) over the Pacific, similar to the GCM's February response. No such reinforcement by the transients occurs for a similar source specified over the eastern Pacific (right panels).

2.4 Understanding and predicting SST variations outside the tropical Pacific

2.4.1 The atmospheric bridge

One example of global climate interaction is the "atmospheric bridge", where atmospheric teleconnections associated with ENSO drive anomalous ocean conditions outside of the equatorial Pacific through changes in the heat, momentum, and fresh water fluxes across the air-sea interface. The resulting SST anomalies can also feed back on the initial atmospheric response to ENSO. As part of the GFDL-Universities Consortium project, we developed a coupled AGCM-mixed layer ocean model and used it to conduct experiments to study the atmospheric bridge and other air-sea interaction processes. In the "MLM" experiment, observed SSTs were prescribed as boundary conditions in the tropical Pacific (15°N–15°S, 172°E–South American Coast), and the remainder of the global oceans were simulated using the variable-depth mixed-layer model. As **Fig. 2.12** shows, the simulated SLP and SST anomalies associated with ENSO are fairly realistic, with stronger cyclonic

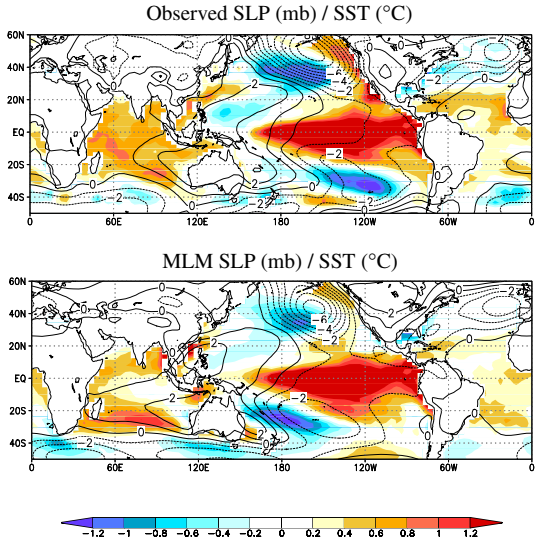

Fig. 2.12. (a) Observed and (b) simulated El Niño minus La Niña composite of SLP (contour interval of 1 mb) and SST (shading interval of 0.2 °C) for DJF(0/1), where 0 indicates the ENSO year and 1 the next year. The composite is based on 9 El Niño and 9 La Niña events during 1950–1999. The observed values are from the NCEP reanalyses and the model results from an average of 16 MLM integrations.

circulation and cold water over the central North and South Pacific and warm water along the west coast of the Americas. ENSO-induced changes in the Walker circulation also lead to warm SSTs in the north tropical Atlantic and Indian Oceans.

How useful is this effect in actually predicting the interannual variations of SSTs outside the tropical Pacific basin? **Figure 2.13** provides one measure of the forecast skill. It shows the correlation of the observed seasonal-mean SST anomalies, over the 50-year 1950–1999 period, with those predicted by the MLM model. The predicted field for each season represents a 16-member ensemble-mean. Results are shown separately for the 50 winter (JFM) and 50 summer (JAS) forecast

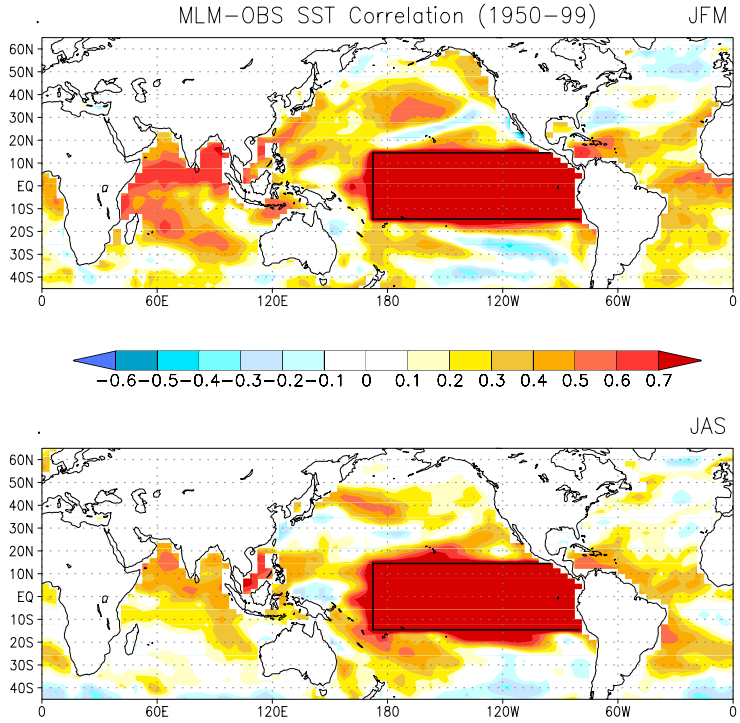

Fig. 2.13. Predictability of seasonal SST anomalies worldwide via the "atmospheric bridge" from the tropical Pacific ocean, in winter (top panel) and summer (bottom panel). Values plotted are the correlations of observed SST anomalies with those predicted by an atmosphere–mixed layer ocean coupled model with specified observed SSTs in the central and eastern tropical Pacific ocean. See text for further details.

cases over which the correlations were calculated. The correlations are generally higher than 0.4 in the central north and south Pacific oceans, and also in the tropical Indian and tropical Atlantic oceans. This is encouraging, and also sheds some light on why the LIM SST forecast models described in section 2.1, that are based solely on SST correlations between different tropical locations, perform as well as they do: the "bridge" effect is implicitly included in them. It is also interesting to compare **Fig. 2.13** with **Fig. 2.12** in areas such as the north Atlantic, where **Fig. 2.12** suggests a bridge effect but **Fig. 2.13** shows it to be unimportant.

2.4.2 The re-emergence of long-lived subsurface temperature anomalies

The atmospheric changes associated with ENSO influence upper-ocean processes that affect the subsurface temperature structure and mixed-layer depth (MLD) long after the ENSO signal decays. Thermal anomalies that form in the surface waters of the extratropics during winter partially reemerge in the following winter, after being sequestered beneath the mixed layer in the intervening summer. SST anomalies generated via the atmospheric bridge recur in the following winter in central North Pacific via this reemergence mechanism (**Fig. 2.14**). The MLD is substantially deeper in the cen-

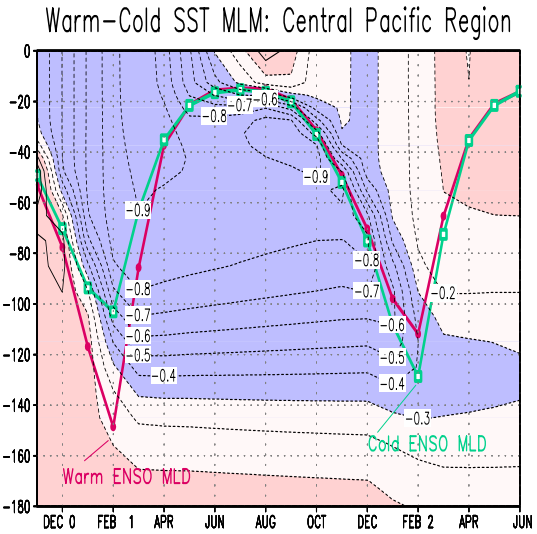

Fig. 2.14 The composite El Niño minus La Niña ocean temperature from Nov(0)–Jun(2) and the composite mixed layer depth (m) during El Niño (red line) and La Niña (blue line) from the MLM experiment in the central North Pacific (180°–160°W, 28°N–42°N).

tral North Pacific during El Niño than La Niña winters, but the reverse is true in the subsequent winter. During El Niño winters, enhanced buoyancy forcing (surface cooling) and mechanical mixing creates a colder and deeper mixed layer. After the MLD shoals in late spring, the cold water stored beneath the surface layer as part of the reemergence process increases the vertical stability of the water column, reducing the penetration of the mixed layer in the following fall and winter.

The reemergence process is not confined to the central North Pacific, nor does it occur solely in conjunction with the atmospheric bridge. **Figure 2.15** shows the evolution of the leading pattern of North Pacific SST variability in observations and in two distinct AGCM – ocean model experiments. In the first experiment, the mixed layer ocean model is active over the entire globe, including the tropical Pacific, and thus does *not* include ENSO. In the second experiment,

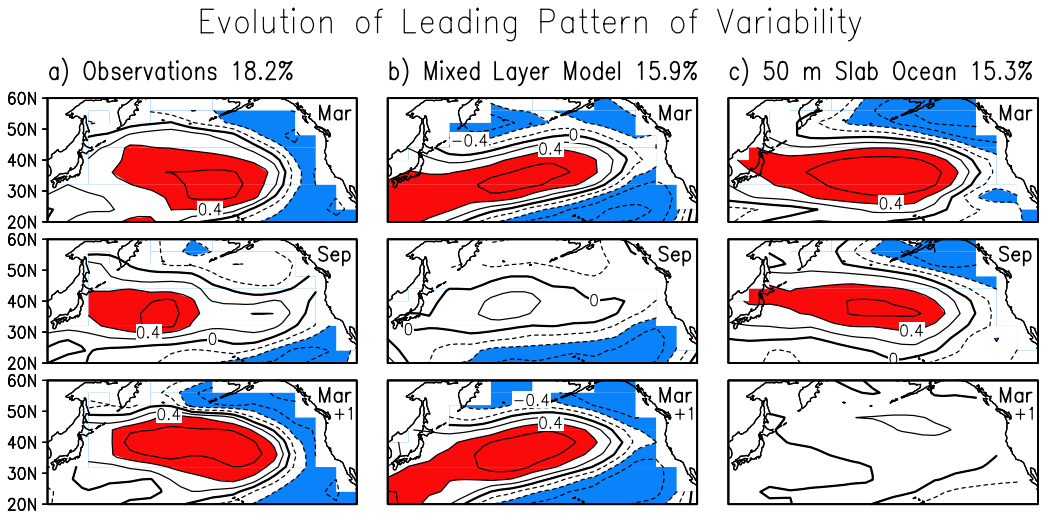

Fig. 2.15. The evolution of the leading pattern of SST variability over 20°N–60°N in the Pacific as indicated by extended EOF analyses of monthly SST anomalies from January through April of the following year. The results are presented as the correlation between the leading principal component (time series of EOF1) with SST anomalies at the individual grid points for March, September and March of the following year. (The other months, which are not shown, indicate a similar evolution). Results are presented for (a) observations for 1950–1995, (b) an AGCM-global MLM simulation, and (c) 4 TOGA-50m slab simulations. The contour interval is 0.2 with values > 0.4 shaded red and those < -0.4 shaded blue.

observed SSTs are specified in the tropical Pacific, but the remainder of the world oceans are simulated by a slab model without mixed-layer physics. The observational column in **Fig. 2.15** shows that the dominant large-scale SST anomaly pattern that forms in the eastern two-thirds of the North Pacific during winter recurs in the following winter without persisting through the intervening summer. Experiment 1 (middle column) reproduces this behavior, but Experiment 2 (right column) does not. These results suggest 1) that the winter-to-winter SST correlations are due to the reemergence mechanism and not due to similar atmospheric forcing of the ocean in consecutive winters, and 2) that the SST anomalies in the tropical Pacific associated with El Niño are not essential for reemergence to occur.

EPILOGUE

Climate variability on seasonal to interannual scales is dominated by the tropical ENSO phenomenon and its global impacts. CDC scientists have been at the forefront in providing evidence that much of the *predictable* evolution of ENSO and its remote atmospheric and oceanic impacts are governed by low-dimensional, linear dynamics. This clarification has proved extremely valuable for basic understanding and for building simple, useful, forecast models. However, it has also raised important new questions. Foremost among these is perhaps that raised by **Figure 2.4**. How much predictability, especially extratropical predictability, exists on this time scale beyond that associated with simple linear ENSO signals? What additional useful predictive information can be extracted by running large GCM ensembles? CDC scientists have addressed these questions by exploring the nonlinearity and sensitivity of the global response to the details of anomalous tropical Pacific SST fields and by focusing on the distributional aspects of the response, especially the changes of variance, rather than just shifts of the mean. We have also contributed to improved understanding of the predictability of SSTs in other ocean basins, through both "atmospheric bridge" and "re-emergence' mechanisms, and the impact of such SSTs on atmospheric predictability. There is encouraging evidence that one will be able to provide substantially improved forecast guidance on this time scale, especially on the tails of the distributions, through better understanding and prediction of these formally second-order but still important effects. The overarching theme of new research in this area must be a community-wide shift from deterministic to probabilistic seasonal predictions. Ultimately, one can extract only so much information from deterministic predictions of a chaotic system. The utility of probabilistic predictions, on the other hand, is unbounded in an important practical sense, in that it is determined to a large degree by the needs of particular users. Future CDC research on this time scale will increasingly reflect this shift of focus to probabilistic predictions, with the climate-society interface and the needs of different categories of user groups in mind.

***Contributed by**: M. Alexander, J. Barsugli, G. Compo, M. Hoerling, S. Peng, C. Penland, and P. D. Sardeshmukh.*